Computed Three-Dimensional Atomic Force Microscopy Images of Biopolymers Using the Jarzynski Equality

THE JOURNAL OF PHYSICAL CHEMISTRY LETTERS
A JOURNAL OF THE AMERICAN CHEMICAL SOCIETY

pubs.acs.org/JPCL

Letter

Computed Three-Dimensional Atomic Force Microscopy Images of Biopolymers Using the Jarzynski Equality

Takashi Sumikama,* Filippo Federici Canova, David Z. Gao, Marcos Penedo, Keisuke Miyazawa, Adam S. Foster, and Takeshi Fukuma*

Cite This: *J. Phys. Chem. Lett.* 2022, 13, 5365−5371

Read Online

ACCESS | Metrics & More | Article Recommendations | Supporting Information

ABSTRACT: Three-dimensional atomic force microscopy (3D-AFM) has resolved three-dimensional distributions of solvent molecules at solid−liquid interfaces at the subnanometer scale. This method is now being extended to the imaging of biopolymer assemblies such as chromosomes or proteins in cells, with the expectation of being able to resolve their three-dimensional structures. Here, we have developed a computational method to simulate 3D-AFM images of biopolymers by using the Jarzynski equality. It is found that some parts of the fiber structure of biopolymers are indeed resolved in the 3D-AFM image. The dependency of 3D-AFM images on the vertical scanning velocity is investigated, and optimum scanning velocities are found. It is also clarified that forces in nonequilibrium processes are measured in 3D-AFM measurements when the dynamics of polymers are slower than the scanning of the probe.

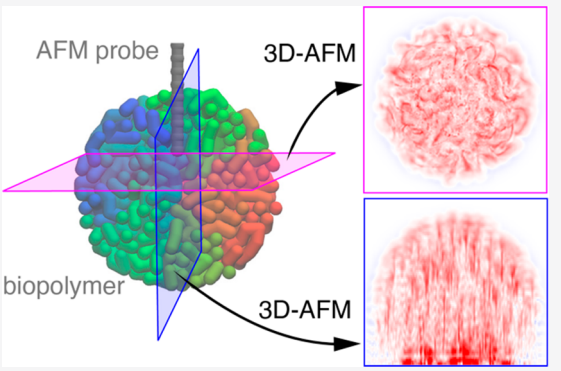

Three-dimensional atomic force microscopy (3D-AFM) is a cutting-edge technology to observe the distributions of solvent molecules at solid−liquid interfaces by mapping forces in 3D space.[1,2] It has been applied to mica,[1,3] lipid membranes,[4] proteins,[5] and DNA surfaces[6] to reveal their interfacial hydration structures. These observations of the average behavior of fluctuating water molecules suggest its capability of observing similar effects in mobile molecular chains in liquids, and there are already a few examples.[4,7,8] A recent paper reported that even the 3D structure of nanostructures in cells has been visualized with specially fabricated thin and long probes.[9] In principle, 3D-AFM technology offers the possibility to resolve the 3D organization of on-surface biopolymers such as chromosomes, cytoskeletons, and so on in cells, whose structures at the nanometer scale are still poorly known. To investigate such possibilities, there is an urgent demand to establish models computing 3D-AFM images of fluctuating biopolymers that can be linked to experiments.

Simulations of 3D-AFM images and a comparison of them with the experiments are essential to provide a theoretical basis for explaining what is resolved in imaging.[10] Accordingly, the simulation techniques to compute 3D-AFM images of solvents on surfaces were developed.[11] The free energy profile was first computed, and then, its derivative gave the so-called mean force to be compared with the measured forces in 3D-AFM experiments. To compute the free energy profile, umbrella sampling[11] and perturbation methods[11,12] were commonly employed. This strategy assumes that the system is in equilibrium throughout a cantilever oscillation cycle, which is only valid for the case where the motions of solvents are much faster than that of the scanning probe. Thus, an alternate method to simulate 3D-AFM images had to be developed for biopolymers since their motions are slower than the scanning velocity.[13]

In our previous paper,[13] we developed a method to visualize the surface topography of biopolymers by calculating the average forces during scanning, but this did not offer any insight into the interactions within the biopolymer necessary to understand 3D-AFM images, which also provide structural information inside the biopolymer. Here, we have developed a method to compute 3D-AFM images of biopolymers by using the Jarzynski equality that relates the work in the nonequilibrium process to the free energy difference.[14] It was recently shown that the Jarzynski equality is capable of estimating free energy even for glassy systems that are not in equilibrium, for which the thermodynamics integration is not applicable.[15] The Jarzynski equality has previously been used to calculate force−distance curves,[16−18] which were compared with the relevant AFM measurements.[19,20] This strategy is extended to map forces in the 3D space even inside biopolymers that are fluctuating in the liquid environments

Received: April 13, 2022
Accepted: May 18, 2022

https://doi.org/10.1021/acs.jpclett.2c01093
J. Phys. Chem. Lett. 2022, 13, 5365−5371

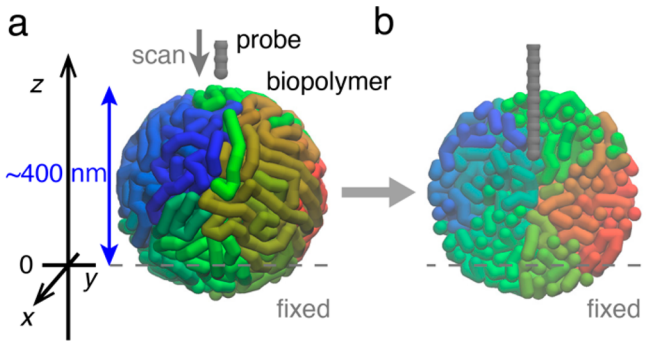

Figure 1. (a) Schematic of the simulation system and AFM probe model. There is one biopolymer composed of 2000 beads (mimicking a chromosome in the interphase) and one AFM probe composed of 50 beads in the system (only part of the probe is shown for clarity). The biopolymer is colored from red (one end) to blue (the other end). (b) A cross section of the biopolymer to illustrate the probe penetrating the polymer (see Movie S1).

(Figure 1), which enables us to see the 3D fiber structures of the polymer. A biopolymer and a probe were simulated using the bead−spring model.[13] The globular structure mimics chromosomes in the interphase (Figure 1a).[21,22] A thin and long probe was used as a model to mimic that used in a recent work;[9] this is long enough to penetrate inside the biopolymer (Figure 1b). The force−distance curves were computed at each x and y position using the Jarzynski equality, and then then all the curves were merged to give a 3D-AFM image (see details in the Supporting Information).

Figure 2a shows the simulation system, and Figure 2b indicates an xz-slice of a 3D-AFM image at the center of polymer. Figure 2c is the color key for the image. The vertical scanning or penetration velocity (v_{scan}) is 1 μm/s in Figure 2. The forces between the penetrating probe and the polymer are weakly attractive (approximately −20 pN) when the probe is outside the polymer, originating from the Lennard-Jones force between the probe and polymer in long-range. On the other hand, the forces when the probe is inside the polymer are repulsive and rapidly increase as the probe approaches the mica surface (where the beads comprising the polymer are constrained). These repulsive forces are attributed to the work pushing the polymer away by the probe during its penetration (see Movie S1 for the pushing motion). The most probable

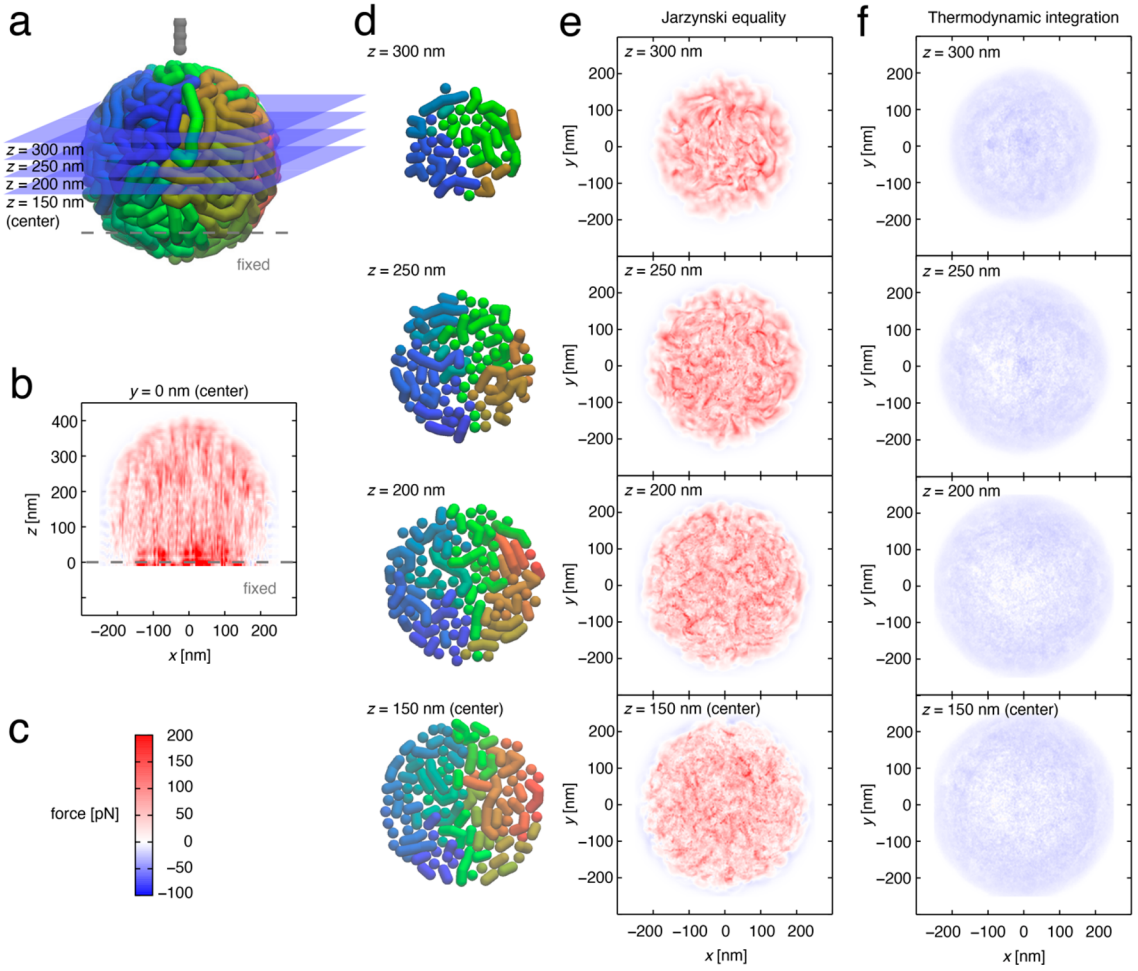

Figure 2. Cross sections of the polymer and simulated 3D-AFM images at v_{scan} = 1 μm/s. (a) The structure of the polymer and four horizontal planes showing the heights of cross sections. (b) An xz-slice (at the center of the polymer) of a simulated 3D-AFM image computed using the Jarzynski equality. Scanned area was 500 nm × 450 nm with 201 × 91 pixels. (c) Color key for the force. (d) Cross sections of the polymer. (e) Four xy-slices of the simulated 3D-AFM image computed using the Jarzynski equality. Scanned area was 500 nm × 500 nm with 201 × 201 pixels. (f) Four xy-slices of the simulated 3D-AFM image computed using thermodynamic integration. Scanned area was 500 nm × 500 nm with 201 × 201 pixels.

https://doi.org/10.1021/acs.jpclett.2c01093
J. Phys. Chem. Lett. 2022, 13, 5365−5371

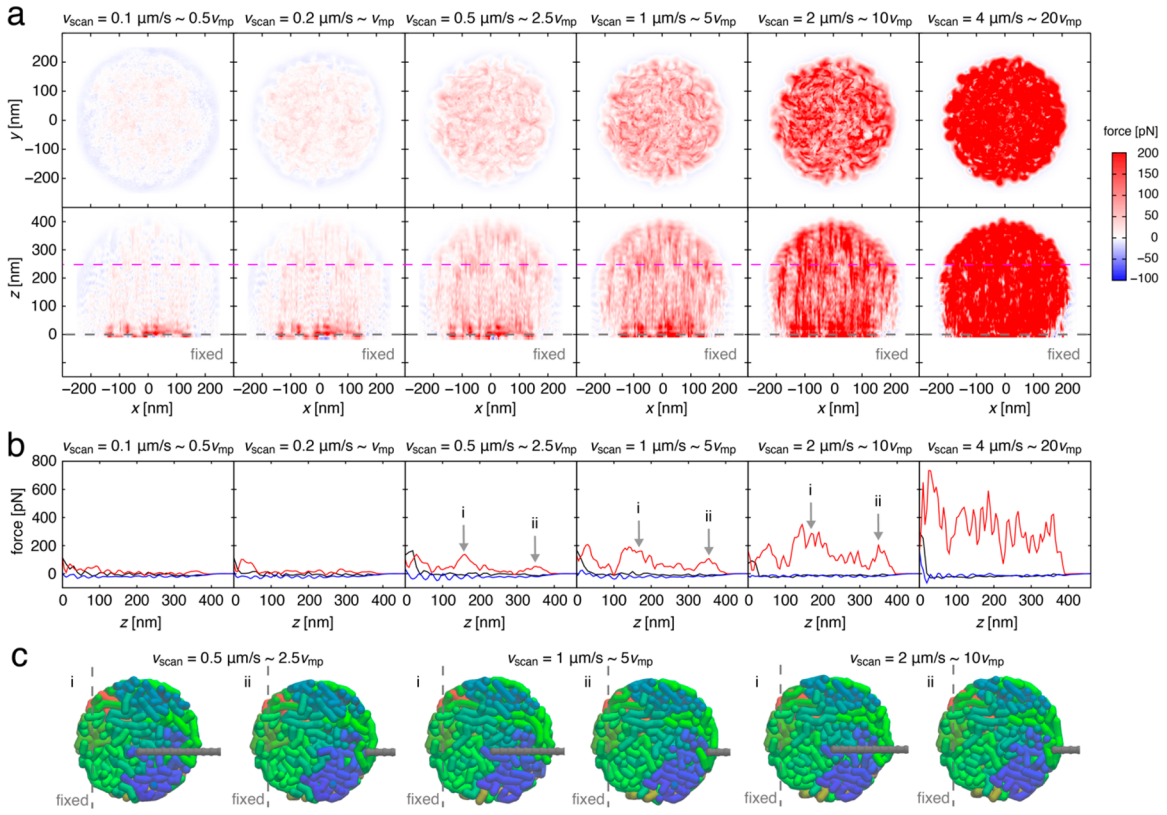

Figure 3. Dependency of 3D-AFM images on the scanning velocity (v_{scan}). (a) *xy*-slices at z = 250 nm and *xz*-slices at the center of the 3D-AFM images. Dashed magenta lines in the bottom indicate the height of *xy*-slice images. (b) The force−distance curves at $x = -50$ and $y = -40$ nm. Red curves are for those obtained using the Jarzynski equality, and black curves are for the thermodynamic integration during the probe approach. Blue curves show the force−distance curve while retracting. (c) Snapshots when large repulsive forces are detected.

speed (v_{mp}) of the beads is calculated by $(2k_BT/m)^{1/2}$, where m is the mass of beads.[23] Using an effective mass accounting for viscosity (m = 0.2 mg),[13] the most probable speed is 0.203 μm/s. Since the motion or configurational relaxation of the polymer is thus slower than the penetrating speed, the probe must displace the polymer out of the way during its penetration. In Figure 2b, we can see several vertical lines (for example, $x = -32.5$ and 50 nm). The movies in which these lines were observed show that the penetrating probe drags the fiber down for a distance where the lines exist (Movie S3 and Movie S4). The probe was also found to push the same parts of fiber down, while the lines are seen (Figure S1). Accordingly, the vertical lines reflect such "dragging". This is also because of the slow relaxation of the polymer: there is insufficient time for the polymer to avoid the penetrating probe.

The sliced images of the polymer at various heights are shown in Figure 2d. The heights where the polymer was cut are indicated by planes in Figure 2a. The relevant *xy*-slices of the 3D-AFM image are shown in Figure 2e. Figure S2 indicates selected parts where fiber structures match 3D-AFM images well, and Movie S5 shows the superimposed movie of Figure 2d,e. Again, the forces on the probe outside the polymer are attractive and repulsive inside. In the *xy*-sliced images, fiber structures are seen in some places. Because of the absence of dragging in the *xy*-direction, there is no vertical (*y*-direction) or horizontal (*x*-direction) lines in the *xy*-slices. Thus, the fiber structure is more clearly seen in *xy*-slices than in *xz*-slices. These fiber structures in force mapping are seen much more clearly in sequential images (Movie S6). In a comparison of these fiber structures in the force mapping (Figure 2e) with the polymer model (Figure 2d), it was found that polymer structures are indeed, but not completely, resolved in the 3D-AFM image (Figure S2 and Movie S5). The structure−force correlation is quantified later.

Figure 2f shows slices of the 3D-AFM image computed using thermodynamic integration. In all images, only weak attractive forces (approximately −15 pN) are seen. In this computation, the probe was stopped at a certain height and the potential energies were sampled and averaged (Movie S2). Most forces acting on the probe, which practically act on the end of the probe, were negative because the polymer and the end of the probe were located in energetically favorable positions during the equilibrium sampling process. This is the reason why attractive forces were observed.

The images computed using thermodynamic integration are completely different from those using the Jarzynski equality, since the work in a nonequilibrium process (pushing away fibers and/or dragging) was not accounted for in thermodynamic integration. Thus, no clear fiber structures are seen. Accordingly, it is significant to simulate 3D-AFM images using the Jarzynski equality in such cases where sample motion is slower than penetration speed, resulting in nonequilibrium work being performed.[15] In other words, forces measured by the AFM experiments in the biological samples whose molecular motions are presumably slower than the probe penetration are not accurately represented by the mean force.

It is known that for certain systems 3D-AFM images (or force−distance curves) change depending on the vertical scanning velocity,[19,24−26] and that the free energy profile

https://doi.org/10.1021/acs.jpclett.2c01093
J. Phys. Chem. Lett. 2022, 13, 5365−5371

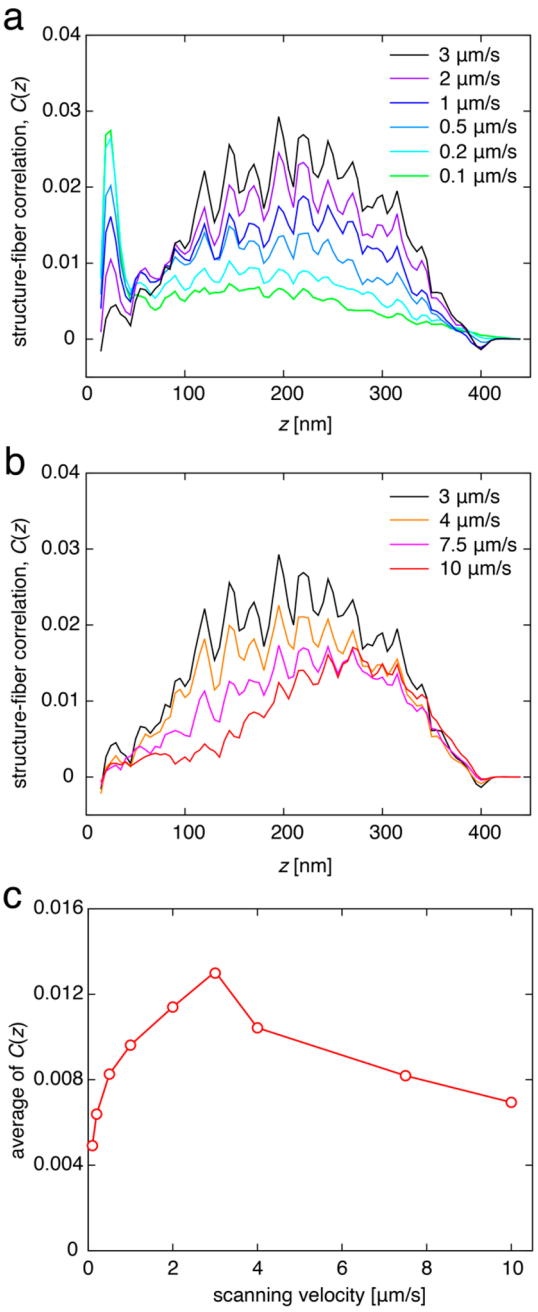

Figure 4. Structure−force correlations at all vertical scanning velocities examined. (a) For $v_{scan} \leq 3$ μm/s. (b) For $v_{scan} \geq 3$ μm/s. (c) Averaged correlation against v_{scan}.

computed by the Jarzynski equality deviates from the potential of mean force evaluated using umbrella sampling when probe velocity is fast.[27−29] As such, 3D-AFM images were additionally simulated at v_{scan} = 0.1 ($\sim 0.5v_{mp}$), 0.2 ($\sim v_{mp}$), 0.5 ($\sim 2.5v_{mp}$), 2 ($\sim 10v_{mp}$), 3 ($\sim 15v_{mp}$), 4 ($\sim 20v_{mp}$), 7.5 ($\sim 36v_{mp}$), and 10 μm/s ($\sim 50v_{mp}$) (see Movie S7 for a comparison of probe penetration and motions of the fiber depending on v_{scan}). The *xy*- and *xz*-slices of 3D-AFM images at six velocities are shown in Figure 3a (see Figure S3 and Movie S8 for at all velocities but with different contrast). It was found that the simulated 3D-AFM images reproduced experimental observations, for example, titin unfolding.[19,24−26] The forces at v_{scan} = 0.1 μm/s ($\sim 0.5v_{mp}$) are so weak that they would be difficult to detect in real experiments. A detectable force is in the range 1−100 pN, depending on the measurement conditions, and is <10 pN for the ideal condition in the dynamic mode.[30,31] At this velocity, the fiber can avoid the penetrating probe, because the scanning velocity is slower than v_{mp} and the forces are close to those obtained by thermodynamic integration (Figure 3b). Even at v_{scan} = 0.2 μm/s ($\sim v_{mp}$), the fiber can still avoid the penetrating probe, resulting in weak forces.

As expected from the Maxwell−Boltzmann distribution, the speeds of almost all beads composing the fiber are less than $2.5v_{mp}$. Accordingly, when $v_{scan} \geq 0.5$ μm/s ($\sim 2.5v_{mp}$), the motion of the fiber is slower than the scanning probe (see Movie S7), and a sufficiently detectable force acts when the probe penetrates the polymer. At v_{scan} = 0.5 μm/s ($\sim 2.5v_{mp}$), we can see some fiber structures in the simulated 3D-AFM image. At v_{scan} = 1 μm/s ($\sim 5v_{mp}$), the image becomes clearer (Figure 3a and Figure S3). The fiber structures are also observed at v_{scan} = 2 μm/s ($\sim 10v_{mp}$) and 3 μm/s ($\sim 15v_{mp}$), while the forces increase (Figure 3a and Figure S3).

Figure 3b shows the force−distance curves. For approaching curves (red lines), we can see that the forces increase when v_{scan} is speeded up. On the other hand, the forces computed by using thermodynamic integration (black lines) are always close to the experimental detection limit and those evaluated by the Jarzynski equality at v_{scan} = 0.1 μm/s, since, as explained, the motions of beads comprising the fiber are faster than v_{scan}. The force−distance curves during retraction were computed by using the Jarzynski equality and are shown by the blue lines. There is no pushing away motion of fibers and dragging in the retracting process, so the force−distance curves have, as expected, no large peak, and there is almost no dependency on v_{scan}.

When the scanning velocity is in the range $2.5v_{mp} \leq v_{scan} \leq 15v_{mp}$, mainly two peaks are seen at ∼160 and ∼360 nm (Figure 3b, see Figure S4 for at all velocities but with different scale). These two peaks (i and ii) originate from dragging and pushing away, respectively (see Figure S4). Thus, they are shared among v_{scan} = 0.5 ($\sim 2.5v_{mp}$), 1 ($\sim 5v_{mp}$), and 2 ($\sim 10v_{mp}$) μm/s (also at v_{scan} = 3 ($\sim 15v_{mp}$) μm/s, Figure S4). Figure 3c shows snapshots when the probe feels a strong repulsion. Irrespective of v_{mp}, the probe pushes away the parts of fiber colored in blue and green at the peaks i and ii, respectively. The peak i is broadened because of the dragging of a part of the fiber colored in blue (Figure S4).

Even at $v_{scan} \geq 4$ μm/s ($\sim 20v_{mp}$), the faster the v_{scan} is, the stronger the forces become (Figure 3a, Figures S3 and S4, and Movie S8). The probe, as mentioned, sometimes cuts the polymer, and the 3D-AFM images were computed before such breaks. When changing the contrast (see Figure S3 and Movie S8), the fiber structures are still seen at v_{scan} = 4 μm/s ($\sim 20v_{mp}$); however, there are some spots of high forces in addition to the fiber. There are cases where peaks in force reflect different fibers, and other cases originate from the dragging (Figure S4). It was found that the dragging increases when v_{scan} is fast (Figure S5). Another reason for high forces is that the probe pushes downward not only a single fiber but also another one behind it (Figure S6). Therefore, the peaks of forces are not well-separated for each fiber. Accordingly, in the force−distance curve at v_{scan} = 4 μm/s (Figure 3b, see Figure S4 for those at v_{scan} = 7.5 and 10 μm/s), there are several peaks in addition to the two main peaks seen in the range 0.5 μm/s $\leq v_{scan} \leq 3$ μm/s. When v_{scan} is 7.5 ($\sim 36v_{mp}$) and 10 ($\sim 50v_{mp}$),

https://doi.org/10.1021/acs.jpclett.2c01093
J. Phys. Chem. Lett. 2022, 13, 5365−5371

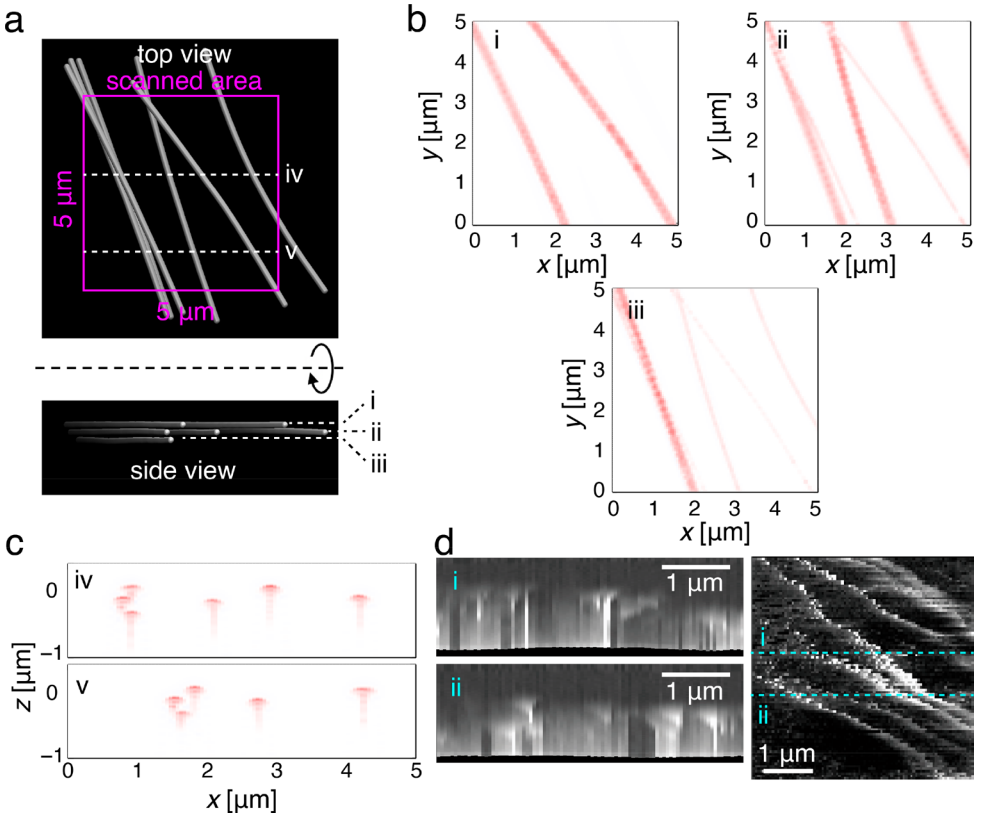

Figure 5. Structure of cytoskeleton fibers and its simulated 3D-AFM images. (a) Top and side views of the simulation system of cytoskeleton fibers. Scanned area is shown by the magenta box. (b) *xy*-slices of the 3D-AFM images at positions i, ii, and iii shown in panel a. Color key for the force is the same as in Figures 2 and 3. (c) *xz*-slices of the 3D-AFM images at positions iv and v shown in panel a. (d) The experimental images of *xz*-slices of the 3D-AFM image of cytoskeleton fibers (left), and an *xz*-slice where the positions of *xy*-slices are shown by dashed cyan lines (right).

the 3D-AFM images become similar to static noise and the fiber structure is difficult to see (Figure S3 and Movie S8).

The structure−force correlation (C) at each height was evaluated by

$$C(z) = \frac{1}{A}\iint \sigma(x, y, z)\frac{F(x, y, z)}{F_{\max}}\mathrm{d}x\mathrm{d}y$$

where A, F, and $F_{\max}$ are the scanned area, forces at each position in 3D space (so the 3D-AFM image), and maximum force in the entire image, respectively. σ is 1 if the position is within 15 nm from the centers of beads and −1 if not, in which the position of the beads was shifted upward by 30 nm since the force is detected approximately 30 nm above the polymer. At $v_{\mathrm{scan}} \geq 4$ μm/s, forces before the probe cut the polymer were used for the analysis, and the area A was changed according to the number of analyzed force−distance curves.

Figure 4 indicates the dependence of the structure−force correlation on v_{scan}. Up to 3 μm/s, the correlation increases when v_{scan} becomes larger (Figure 4a). Further increase of v_{scan}, however, decreases the correlation because of the static noise (Figure 4b). Accordingly, the 3D-AFM image best matches the polymer coordinates at v_{scan} = 3 μm/s (∼15v_{mp}) (Figure 4c). Thus, there exists an optimum velocity range for vertical scan, and the force curve would reflect a rather detailed fiber structure when the scanning velocity is adequately adjusted.

Lastly, a comparison with the experiment in which the 3D organization of cytoskeletal fibers was visualized by 3D-AFM measurements[9] is shown. This is the best example for comparison because both the actual structure and the 3D-AFM image are known. In the 3D-AFM image of cytoskeleton fibers (Figure 3C,D in ref 9), we can see high force regions running up and down in 3D space, reflecting the structure of the cytoskeleton fibers. Note that these images were processed to reduce the forces that originated by dragging. We mimicked the straight fiber structure by increasing the stiffness (Figure 5a) and computed its 3D-AFM image (see Supporting Information for details of the method). In the successive *xy*-slices of the 3D-AFM image from higher to lower positions (Figure 5b and Movie S9), regions of high force appear in sequence according to their heights as in the experiments. In the sliced image of lower position, the afterimages of fibers in the higher position appear as weaker forces because of dragging. In the *xz* slice of the 3D-AFM image (Figure 5c), elongated triangles are visible. This shape reflects the position of fibers and the dragging afterward while the nanoprobe is moving down. The triangular shape is caused by the finite diameter of the probes, which laterally touches the fiber even when it is not perfectly on the center of the fiber. The dragging strength decreases as the probe moves away from the center (Figure S8). These characteristic triangles are also seen in the experimental images before the force reduction process (Figure 5d). The forces computed using the thermodynamic integration are very weak (<5 pN) and are usually negative as in the case of the globular structure (Figure S9). Compared to the 3D-AFM image using the thermodynamic integration, the 3D-AFM image using the Jarzynski equality is closer to the experimental image. A remarkable difference between Figure 5c,d is a reversed contrast. In the simulation, the force is larger when the probe contacts the fiber and less during dragging

https://doi.org/10.1021/acs.jpclett.2c01093
J. Phys. Chem. Lett. 2022, 13, 5365−5371

after laterally moving the fiber. In the experiment, on the other hand, the signal is weak above the fiber and gets stronger as the probe pushes the fiber downward. A plausible explanation is that cytoskeleton fibers in cells are attached to the cell membrane, and thus, the force would become larger while the probe pushes the fiber downward due to the interaction between fiber and membrane. However, such an interaction is not implemented on the simulation. Therefore, for relatively stiff straight fibers, the method developed here shows some qualitative agreement with the experiment, although the force magnitude during dragging is different.

In conclusion, we developed a method to compute 3D-AFM images of biopolymers using the Jarzynski equality. Our simulation demonstrated that 3D-AFM technology is even capable of resolving fluctuating biopolymers: some fiber structures were clearly observed in the simulated 3D-AFM images. This supports previous 3D-AFM measurements observing molecular chains.[4,7,8] The computed forces increased when the scanning velocity becomes fast, which qualitatively reproduced force-scanning velocity relations in some experiments.[19,24−26] Moreover, the optimum scanning velocity was found in the range of several to 10 times faster than the most probable speed of the biopolymer. It was found that the use of thermodynamic integration to compute force−distance curves and 3D-AFM images is unsuitable when the motions of the samples are slower than the penetration speed of the AFM probe, because the system is far from thermodynamic equilibrium. It is expected that the motions of biomolecules are relatively slow; thus, the forces measured in the AFM measurements of biomolecules would be forces in a non-equilibrium process rather than the so-called mean force. The method developed here is applicable to various fibers in cells such as DNA and so on by changing parameters such as stiffness, providing an important theoretical base for such experimental measurements. As an example, it was applied for cytoskeleton fibers to be compared with recent experiments.[9] Another important issue for the near future is to establish a method to convert 3D-AFM images to actual fiber structures in order to utilize 3D-AFM imaging as a tool to reveal structures of biopolymers. For this, AI using machine learning or some image analysis technologies are expected to help.

■ ASSOCIATED CONTENT

Supporting Information

The Supporting Information is available free of charge at https://pubs.acs.org/doi/10.1021/acs.jpclett.2c01093.

Simulation details and figures showing additional results such as fiber sturcture comparisons, velocities of beads of the fiber, and force−distance curves (PDF)

Movie of probe penetration into the biopolymer (Movie S1) (MP4)

Simulation during the thermodynamic integration (Movie S2) (MP4)

Force−distance curve at $x = -32.5$ nm and a movie of probe penetration (Movie S3) (MP4)

Force−distance curve at $x = 50$ nm and a movie of probe penetration (Movie S4) (MP4)

Superimposed movies of fiber structure and 3D-AFM images (Movie S5) (MP4)

3D-AFM image at $v_{scan} = 1$ μm/s (Movie S6) (MP4)

Probe penetrating movies at different scanning velocities (Movie S7) (MP4)

3D-AFM images at different scanning velocities (Movie S8) (MP4)

3D-AFM image of cytoskeleton fibers (Movie S9) (MP4)

■ AUTHOR INFORMATION

Corresponding Authors

Takashi Sumikama − *PRESTO, JST, Kawaguchi, Saitama 332-0012, Japan; Nano Life Science Institute (WPI-NanoLSI), Kanazawa University, Kanazawa 920-1192, Japan;* orcid.org/0000-0003-3696-5720; Email: sumi@staff.kanazawa-u.ac.jp

Takeshi Fukuma − *Nano Life Science Institute (WPI-NanoLSI), Kanazawa University, Kanazawa 920-1192, Japan; Division of Electrical Engineering and Computer Science, Kanazawa University, Kanazawa 920-1192, Japan;* orcid.org/0000-0001-8971-6002; Email: fukuma@staff.kanazawa-u.ac.jp

Authors

Filippo Federici Canova − *Nanolayers Research Computing Ltd., London N12 0HL, United Kingdom; Department of Applied Physics, Aalto University, Aalto 00076, Finland*

David Z. Gao − *Nanolayers Research Computing Ltd., London N12 0HL, United Kingdom; Department of Physics, Norwegian University of Science and Technology (NTNU), 7491 Trondheim, Norway*

Marcos Penedo − *Nano Life Science Institute (WPI-NanoLSI), Kanazawa University, Kanazawa 920-1192, Japan; Laboratory for Bio and Nanoinstrumentation, Institute for Bioengineering, École Polytechnique Fédérale de Lausanne, Lausanne CH-1015, Switzerland;* orcid.org/0000-0002-2936-7354

Keisuke Miyazawa − *Nano Life Science Institute (WPI-NanoLSI), Kanazawa University, Kanazawa 920-1192, Japan; Division of Electrical Engineering and Computer Science and Faculty of Frontier Engineering, Kanazawa University, Kanazawa 920-1192, Japan;* orcid.org/0000-0002-5012-8040

Adam S. Foster − *Nano Life Science Institute (WPI-NanoLSI), Kanazawa University, Kanazawa 920-1192, Japan; Department of Applied Physics, Aalto University, Aalto 00076, Finland;* orcid.org/0000-0001-5371-5905

Complete contact information is available at: https://pubs.acs.org/10.1021/acs.jpclett.2c01093

Author Contributions

T.S. and T.F. conceived the work. T.S. developed program code, performed simulations, and visualized models. T.S., F.F.C., D.Z.G., A.S.F., and T.F. analyzed data. M.P. and K.M. performed 3D-AFM experiments. A.S.F. and T.F. supervised. T.S. drafted the manuscript, and all the authors reviewed and edited.

Notes

The authors declare no competing financial interest.

■ ACKNOWLEDGMENTS

The calculation was carried out on the supercomputers at the Research Center for Computational Science in Okazaki, Japan (Project: 21-IMS-C114, 22-IMS-C114). T.S. is grateful to Dr. Sumino (Kanazawa Univ.) for fruitful discussion. This work was supported by World Premier International Research

Center Initiative (WPI), MEXT, Japan, JST, PRESTO (JPMJPR20K6), Japan, and WPI-NanoLSI Transdisciplinary Research Promotion Grant from Kanazawa University; JSPS KAKENHI (19K22125 and 20H00345); and JST Mirai-Project (18077272). A.S.F. was supported by the Academy of Finland (314862).

■ ABBREVIATIONS

AFM, atomic force microscopy; 3D-AFM, three-dimensional atomic force microscopy

■ REFERENCES

(1) Fukuma, T.; Ueda, Y.; Yoshioka, S.; Asakawa, H. Atomic-scale distribution of water molecules at the mica-water interface visualized by three-dimensional scanning force microscopy. *Phys. Rev. Lett.* **2010**, *104*, 016101.

(2) Fukuma, T.; Garcia, R. Atomic- and Molecular-Resolution Mapping of Solid-Liquid Interfaces by 3D Atomic Force Microscopy. *ACS Nano* **2018**, *12*, 11785−11797.

(3) Kobayashi, K.; Oyabu, N.; Kimura, K.; Ido, S.; Suzuki, K.; Imai, T.; Tagami, K.; Tsukada, M.; Yamada, H. Visualization of hydration layers on muscovite mica in aqueous solution by frequency-modulation atomic force microscopy. *J. Chem. Phys.* **2013**, *138*, 184704.

(4) Asakawa, H.; Yoshioka, S.; Nishimura, K.; Fukuma, T. Spatial Distribution of Lipid Headgroups and Water Molecules at Membrane/Water Interfaces Visualized by Three-Dimensional Scanning Force Microscopy. *ACS Nano* **2012**, *6*, 9013−9020.

(5) Herruzo, E. T.; Asakawa, H.; Fukuma, T.; Garcia, R. Three-dimensional Quantitative Force Maps in Liquid with 10 Piconewton, Angstrom and Sub-minute Resolutions. *Nanoscale* **2013**, *5*, 2678−2685.

(6) Kuchuk, K.; Sivan, U. Hydration Structure of a Single DNA Molecule Revealed by Frequency-Modulation AFM. *Nano Lett.* **2018**, *18*, 2733−2737.

(7) Molino, P. J.; Yang, D.; Penna, M.; Miyazawa, K.; Knowles, B. R.; MacLaughlin, S.; Fukuma, T.; Yarovsky, I.; Higgins, M. J. Hydration Layer Structure of Biofouling-Resistant Nanoparticles. *ACS Nano* **2018**, *12*, 11610−11624.

(8) Ikarashi, T.; Yoshino, T.; Nakajima, N.; Miyata, K.; Miyazawa, K.; Morais Jaques, Y.; Foster, A. S.; Uno, M.; Takatoh, C.; Fukuma, T. Inhibition of Silica Nanoparticle Adhesion to Poly(vinyl alcohol) Surfaces by Ammonia-Mediated Hydration: Implications for Effective Post-Chemical-Mechanical Planarization Cleaning. *ACS Appl. Nano Mater.* **2021**, *4*, 71−83.

(9) Penedo, M.; Miyazawa, K.; Okano, N.; Furusho, H.; Ichikawa, T.; Alam, M. S.; Miyata, K.; Nakamura, C.; Fukuma, T. Visualizing intracellular nanostructures of living cells by nanoendscopy-AFM. *Sci. Adv.* **2021**, *7*, No. eabj4990.

(10) Fukuma, T.; Reischl, B.; Kobayashi, N.; Spijker, P.; Canova, F. F.; Miyazawa, K.; Foster, A. S. Mechanism of Atomic Force Microscopy Imaging of Three-Dimensional Hydration Structures at a Solid-Liquid Interface. *Phys. Rev. B: Condens. Matter Mater. Phys.* **2015**, *92*, 155412.

(11) Reischl, B.; Watkins, M.; Foster, A. S. Free Energy Approaches for Modeling Atomic Force Microscopy in Liquids. *J. Chem. Theory Comput.* **2013**, *9*, 600−608.

(12) Watkins, M.; Shluger, A. L. Mechanism of Contrast Formation in Atomic Force Microscopy in Water. *Phys. Rev. Lett.* **2010**, *105*, 196101.

(13) Sumikama, T.; Foster, A. S.; Fukuma, T. Computed Atomic Force Microscopy Images of Chromosomes by Calculating Forces with Oscillating Probes. *J. Phys. Chem. C* **2020**, *124*, 2213−2218.

(14) Jarzynski, C. Nonequilibrium equality for free energy differences. *Phys. Rev. Lett.* **1997**, *78*, 2690−2693.

(15) Vinutha, H. A.; Frenkel, D. Estimation of the equilibrium free energy for glasses using the Jarzynski equality. *J. Chem. Phys.* **2021**, *154*, 231101.

(16) Hummer, G.; Szabo, A. Free energy reconstruction from nonequilibrium single-molecule pulling experiments. *Proc. Natl. Acad. Sci. U. S. A.* **2001**, *98*, 3658−3661.

(17) Lee, E. H.; Hsin, J.; Sotomayor, M.; Comellas, G.; Schulten, K. Discovery through the computational microscope. *Structure* **2009**, *17*, 1295−1306.

(18) Vilhena, J. G.; Pimentel, C.; Pedraz, P.; Luo, F.; Serena, P. A.; Pina, C. M.; Gnecco, E.; Pérez, R. Atomic-Scale Sliding Friction on Graphene in Water. *ACS Nano* **2016**, *10*, 4288−4293.

(19) Rico, F.; Gonzalez, L.; Casuso, I.; Puig-Vidal, M.; Scheuring, S. High-Speed Force Spectroscopy Unfolds Titin at the Velocity of Molecular Dynamics Simulations. *Science* **2013**, *342*, 741−743.

(20) Raman, S.; Utzig, T.; Baimpos, T.; Ratna Shrestha, B.; Valtiner, M. Deciphering the scaling of single-molecule interactions using Jarzynski's equality. *Nat. Commun.* **2014**, *5*, 5539.

(21) Alberts, B.; Johnson, A.; Lewis, L.; Morgan, D.; Raff, M.; Roberts, K.; Walter, P. *Molecular Biology of the Cell*, 6th ed.; Garland Science, 2014.

(22) Lieberman-Aiden, E.; van Berkum, N. L.; Williams, L.; Imakaev, M.; Ragoczy, T.; Telling, A.; Amit, I.; Lajoie, B. R.; Sabo, P. J.; Dorschner, M. O.; Sandstrom, R.; Bernstein, B.; Bender, M. A.; Groudine, M.; Gnirke, A.; Stamatoyannopoulos, J.; Mirny, L. A.; Lander, E. S.; Dekker, J. Comprehensive Mapping of Long-Range Interactions Reveals Folding Principles of the Human Genome. *Science* **2009**, *326*, 289−293.

(23) Atkins, P.; de Paula, J.; Keeler, J. *Atkins' Physical Chemistry*, 11th ed.; Oxford University Press, 2018.

(24) *Atomic Force Microscopy in Cell Biology*, Jena, B. P., Hörber, J. K. H., Eds.; Academic Press, 2002.

(25) Yuan, C.; Chen, A.; Kolb, P.; Moy, V. T. Energy landscape of streptavidin-biotin complexes measured by atomic force microscopy. *Biochemistry* **2000**, *39*, 10219−10223.

(26) Baumgartner, W.; Hinterdorfer, P.; Ness, W.; Raab, A.; Vestweber, D.; Schindler, H.; Drenckhahn, D. Cadherin interaction probed by atomic force microscopy. *Proc. Natl. Acad. Sci. U. S. A.* **2000**, *97*, 4005−4010.

(27) Park, S.; Khalili-Araghi, F.; Tajkhorshid, E.; Schulten, K. Free Energy Calculation from Steered Molecular Dynamics Simulations Using Jarzynski's Equality. *J. Chem. Phys.* **2003**, *119*, 3559−3566.

(28) Perišić, O.; Lu, H. On the Improvement of Free-Energy Calculation from Steered Molecular Dynamics Simulations Using Adaptive Stochastic Perturbation Protocols. *PLoS One* **2014**, *9*, No. e101810.

(29) Noh, S. Y.; Notman, R. Comparison of umbrella sampling and steered molecular dynamics methods for computing free energy profiles of aromatic substrates through phospholipid bilayers. *J. Chem. Phys.* **2020**, *153*, 034115.

(30) Fukuma, T; Onishi, K; Kobayashi, N; Matsuki, A; Asakawa, H Atomic-resolution imaging in liquid by frequency modulation atomic force microscopy using small cantilevers with megahertz-order resonance frequencies. *Nanotechnology* **2012**, *23*, 135706.

(31) Fukuma, T. Improvements in fundamental performance of in-liquid frequency modulation atomic force microscopy. *Microscopy* **2020**, *69*, 340−349.

https://doi.org/10.1021/acs.jpclett.2c01093
J. Phys. Chem. Lett. 2022, 13, 5365−5371